Anal. Chem. **2008,** *80,* 1689−1695

Chemical Reaction Imaging within Microfluidic Devices Using Confocal Raman Spectroscopy: The Case of Water and Deuterium Oxide as a Model System

Flavie Sarrazin and Jean-Baptiste Salmon*

LOF, Unité mixte CNRS−Rhodia−Bordeaux 1, 178 avenue du Docteur Schweitzer, F-33608 Pessac cedex, France

David Talaga and Laurent Servant

Université Bordeaux 1, ISM, 351 cours de la Libération, 33405 Talence-cedex, France

Microfluidic devices face presently a tremendous interest, especially for the development of labs-on-a-chip systems. One of the primary challenges for such applications is the ability to perform local chemical detection and analysis from various species. In this paper, we investigate the use of confocal Raman spectroscopy from both qualitative and quantitative sides, to obtain spatially resolved concentration maps of chemically reactive fluids flowing in different channels networks. As a model chemical reaction, we used the isotopic exchange reaction between D_2O and H_2O, which is diffusion-controlled and whose equilibrium states exhibit distinct Raman signatures depending on the composition. Two types of chip technologies were studied, which are typical of those used for chemical kinetics investigations. In the first one, reagent mixing occurs by molecular interdiffusion of the two streams (H_2O and D_2O) flowing side by side in the same channel; in the second one, reagents are hosted in droplets moving in winding channels that enhance the mixing. In the first series of experiments, we were able to extract Raman images of H_2O, D_2O, and HOD concentrations in the main channel together with an estimate of an interdiffusion coefficient, and in the second one, we evidenced the influence of channel wiggles on mixing efficiency.

Microfluidics covers a wide range of technologies and methods that allow the control of fluid flows in small complex geometries.[1,2] Such technologies, namely, with the development of the so-called lab-on-a-chip,[3] have proved to be successful to perform high-throughput biological assays,[4] chemical synthesis,[5] and rate constants measurements[6,7] In this context, investigating chemical reactions in microfluidic geometries offers several advantages, such as efficient thermal transfers,[8] fast fluid mixing,[9,10] and opportunities for continuous measurements,[11,12] providing the coupling of microfluidic systems with local analytical probes is made possible and straightforward.

A fruitful strategy relies on collecting maps of the local repartitions of the chemical species within these microfluidic systems. Indeed, because such devices operate mostly in stationary conditions, mapping species repartition offers significant insights in kinetics and reaction schemes of chemical reactions. Among the analytical techniques that have the required spatial resolution to explore microsystems (typically in the μm range), optical spectroscopic techniques are of great interest. For example, the use of optical confocal microscopy offers the opportunity to isolate the signal originating from a micrometer-sized volume, eliminating the main contributions of out-of-focus signals. It thus becomes possible to obtain the spatial distribution of various components by mapping separately a judicious selection of nonoverlapping optical signals (fluorescence, Raman, absorption), typical of the species of interest. Several spectroscopic techniques have been coupled to microfluidics to perform such local analysis; among which, Raman spectroscopy offers great perspectives to investigate chemical reactions. These pioneering previous works have demonstrated that Raman spectroscopy may be useful to perform in situ monitoring of chemical reactions [13−16] and chemical

* To whom correspondence should be addressed. E-mail: Jean-Baptiste-.Salmon-exterieur@eu.rhodia.com.

(1) Squires, T. M.; Quake, S. R. *Rev. Mod. Phys.* **2005**, *77*, 977.
(2) Stone, H. A.; Stroock, A. D.; Ajdari, A. *Annu. Rev. Fluid Mech.* **2004**, *36*, 381.
(3) Vilkner, T.; Janasek, D.; Manz, A. *Anal. Chem.* **2004**, *76*, 3373.
(4) Thorsen, T.; Maerkl, S. J; Quake, S. R. *Science* **2002**, *298*, 580
(5) Song, H.; Tice, J. D.; Ismagilov, R. F. *Angew. Chem., Int. Ed.* **2003**, *42*, 767.
(6) Song, H.; Ismagilov, R. F. *J. Am. Chem. Soc.* **2003**, *125*, 14613.
(7) Salmon, J.-B.; Dubrocq, C.; Tabeling, P.; Charier, S.; Alcor, D. Jullien, L.; Ferrage, F. *Anal. Chem.* **2005**, *77*, 3417.
(8) Dummann, G.; Quittmann, U.; Groschel, L.; Agar, D. W.; Worz, O.; Morgenchweiss, K. *Catal. Today* **2003**, *79*, 433.
(9) Knight, J. B.; Vishwanath, A.; Brody, J. P.; Austin, R. H. *Phys. Rev. Lett.* **1998**, *80*, 3863.
(10) Pabit, A.; Hagen, S. *Biophys. J.* **2002**, *83*, 2872.
(11) Joanicot, M.; Ajdari, A. *Science* **2005**, *309*, 887.
(12) DeMello, J. *Nature* **2006**, *44*, 394.
(13) Lee, M.; Lee, J.-P.; Rhee, H.; Choo, J.; Chai, Y. G.; Lee, E. K. *J. Raman Spectrosc.* **2003**, *34*, 737.
(14) Fletcher, P.; Haswell, S.; Zhang, X. *Electrophoresis* **2003**, *24*, 3239.
(15) Barnes, S. E.; Cygan, Z. T.; Yates, J. K.; Beers, K. L.; Amis, E. J. *Analyst* **2006**, *131*, 1027.

10.1021/ac7020147 CCC: $40.75
Published on Web 01/29/2008

separations,[19] reaction optimization,[18] kinetics of protein folding measurements,[21] and surface-enhanced Raman scattering (SERS) detection for quantitative analysis.[17,20] Recently, we have used Raman confocal microscopy to image the interdiffusion zone of two nonreacting pure liquids diffusing side by side in a microchannel[22] and fluid mixing within droplets flowing in a straight microchannel.[23] In the present work, we use Raman spectroscopy to acquire Raman images of interdiffusion within a chemical reaction in two different microfluidic devices, poly(dimethylsiloxane) (PDMS) and glass/silicon chips, and for these two different mixing strategies: laminar diffusion between two coflowing streams, and convective mixing inside droplets flowing in a silicone oil stream. In this report, we thus extend our previous works to the more general case of the mixing of species within a chemical reaction occurring in different microfluidic geometries, and we propose an original method to extract quantitative concentration fields of the chemical compounds and also remove the Raman contributions of the silicone oil stream in the case of the droplet-based flow.

The model chemical reaction we selected is an isotopic substitution involving simple molecules:

$$H_2O + D_2O \leftrightharpoons 2\,HOD$$

This reaction has been extensively studied; reactants are widely available, are not corrosive, and can be used in all types of microfluidic devices. Furthermore, this system is well suited for spectroscopic investigations: upon isotope replacement, a frequency shift is produced for any vibration that involves appreciable movement of the exchanged atom, and the larger the isotopic mass difference, the greater the frequency shift is. Consequently, $H_2O/D_2O/HOD$ mixtures have distinct vibrational signatures depending on the molar fractions and, thus, on their composition.[24] The above reaction is also diffusion-controlled, and the HOD spatial repartition is dominated by the interdiffusion of H_2O and D_2O within the microfluidic system. Two common microfluidic geometries were investigated: the interdiffusion of H_2O and D_2O streams flowing side by side in a glass−silicon microchannel, and the mixing inside microreactors formed by the coalescence of droplets containing H_2O and D_2O carried by a silicone oil stream, in a PDMS device. These two microfluidic devices differ by the reactants' mixing time they provide. In the first one, mixing happens only by molecular diffusion, whereas in the second device, mixing occurs by convection and molecular diffusion within the droplets. In the first case, we managed to map the interdiffusion process and to extract an interdiffusion coefficient related to this reaction. In the second case, we showed that simple data analysis allows us to remove the contribution of the silicone oil signal to the recorded Raman spectra and, therefore, to obtain Raman images of the species mixing within the droplets.

MATERIALS AND METHODS

A. Model Reaction Investigated: $H_2O + D_2O \leftrightharpoons 2HOD$. The kinetics of the isotopic exchange reaction being very fast, the chemical equilibrium is reached instantaneously at each location in the microreactor. The local concentrations are therefore related to the equilibrium constant through $[HOD]^2 = K_e[H_2O][D_2O]$, where $K_e = 3.88$ is the equilibrium constant at room temperature.[25] Let ψ be the initial molar fraction of D_2O mixed with pure water. When complete mixing is performed, the equilibrium molar fractions of H_2O, D_2O, and HOD are given respectively by $1 - \psi - \phi/2$, $\psi - \phi/2$, and ϕ, where ϕ is simply obtained from

$$K_e = \frac{\phi^2}{(\psi - \phi/2)(1 - \psi - \phi/2)} \quad (1)$$

The vibrational frequencies associated with hydrogen motion in liquid water occur in the region of 3500 cm^{-1} for OH stretching modes (2500 cm^{-1} for D_2O) and 1650 cm^{-1} for HOH bending modes (1200 cm^{-1} for D_2O). The bending modes have a weaker Raman intensity as compared to the stretching modes. The precise assignment of the Raman spectra of pure and isotopic H_2O/D_2O mixtures may be rather complex. In these solutions, OD and OH oscillators vibrate according to their local surroundings, and their bands display various features associated with the different local structures of the liquid. It is beyond the scope of this paper to provide a detailed analysis of the spectroscopic details of such mixtures (see ref 24 for more details). We restrict our attention to the OH/OD spectral stretching region in order to probe the species concentrations within the mixture from the measured Raman spectra.

Figure 1a reports the Raman spectra of pure H_2O and pure D_2O solutions, and of an isotopic molar mixture of H_2O and D_2O ($\psi = 0.478$). Such Raman spectra were acquired using a commercial spectrometer (LabRam HR, Jobin-Yvon, acquisition time 20 s, grating 1800 cm^{-1}, spectral resolution 1 cm^{-1}, incident wavelength 514.5 nm). We can notice that, for pure H_2O and D_2O solutions, ν_{OH} and ν_{OD} stretching modes exhibit simplified profiles with two components at $\nu_{sym} = 2500$ and $\nu_{asym} = 2400$ cm^{-1} for D_2O, and at $\nu_{sym} = 3420$ and $\nu_{asym} = 3260$ cm^{-1} for H_2O. In the case of the H_2O/D_2O mixture, the principal Raman intensity maximums are observed at 2500 and 3420 cm^{-1} and refer to OH and OD stretching vibrations of D_2O, H_2O, and HOD. The observed profile of these bands is of course closely related to the mixture composition.

B. Composition Calibration from Raman Spectra. Raman reference spectra of H_2O/D_2O solutions corresponding to various ψ values were recorded and reported in Figure 1b. These data clearly show that one can extract the molar fractions of the three

(16) Park, T.; Lee, M.; Choo, J.; Kim, Y. S.; Lee, E. K.; Kim, D. J.; Lee, S.-H. *Appl. Spectrosc.* **2004**, *58*, 1172.
(17) Strehle, K. R.; Cialla, D.; Rosch, P.; Henkel, T.; Kohler, M.; Popp, J. *Anal. Chem.* **2007**, *79*, 1542
(18) Leung, S. A.; Winkle, R. F.; Wootton, R. C.; deMello, A. J. *Analyst* **2005**, *130*, 46
(19) Walker, P. A.; Morris, M. D.; Burns, M. A.; Johnson, B. N. *Anal. Chem.* **1998**, *70*, 3766.
(20) Jung, J.; Choo, J.; Kim, D. J.; S. Lee, *Bull. Korean Chem. Soc.* **2007**, *27*, 277.
(21) Pan, D.; Ganim, Z.; Kim, J. E.; Verhoeven, M. A.; Lugtenburg, J.; Mathies, R. *J. Am. Chem. Soc.* **2002**, *124*, 4857.
(22) Salmon, J.-B.; Ajdari, A.; Tabeling, P.; Servant, L.; Talaga, D.; Joanicot, M. *Appl. Phys. Lett.* **2005**, *86*, 094106.
(23) Cristobal, G.; Arbouet, L.; Sarrazin, F.; Talaga, D.; Bruneel, J.-L. Joanicot, M.; Servant, L. *Lab Chip* **2006**, *6*, 1140.
(24) Rull, F. *Pure Appl. Chem.* **2002**, *74*, 1859.
(25) Libnau, F. O.; Christy, A. A.; Kvalheim, O. M. *Appl. Spectrosc.* **1995**, *49*, 1431.

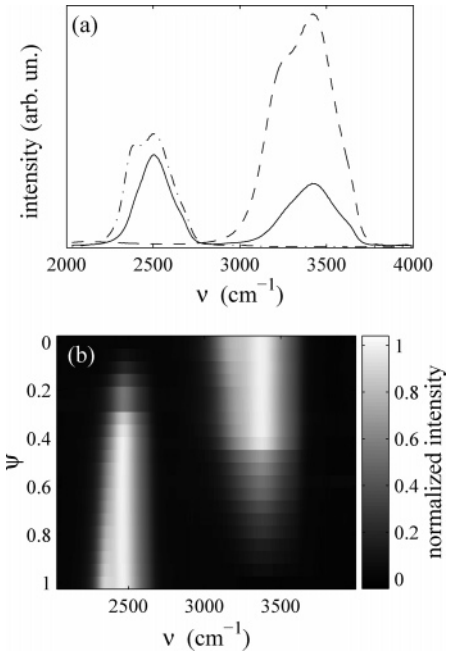

Figure 1. (a) Raman spectra of pure H_2O (dashed line), of pure D_2O (dashed−dotted line), and of a mixture corresponding to $\psi = 0.478$, i.e. 0.230, 0.272, and 0.495 for the molar fractions of H_2O, D_2O, and HOD, respectively (continuous line). (b) Map of the Raman spectra for different initial molar fractions ψ of D_2O. Each spectrum has been normalized by its maximal intensity.

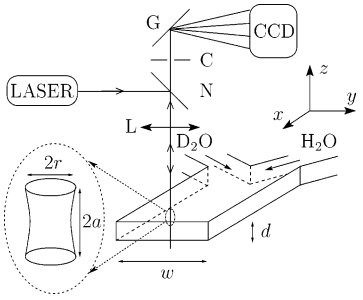

Figure 2. Instrumental setup. L denotes the objective, N the notch filter, C the confocal pinhole, and G the grating. *a* and *r* are the geometrical dimensions of the confocal volume determined by the objective and the size of the confocal pinhole. The main channel is $w = 500$ μm wide and $d = 40$ μm high.

compounds of a mixture of unknown composition (ψ unknown), by comparison of its Raman spectrum with these reference spectra and using eq 1. Indeed, by normalizing the spectra, it is possible using a simple least-squares method to extract from one measured Raman spectrum, the corresponding molar fractions of the mixture with a correct resolution (±1%) providing an extrapolation of the two-dimensional data displayed in Figure 1b. Note that the shape of the spectrum is sufficient to perform such an analysis (when the same normalization is applied to the spectra).

C. Microfluidic Geometries. Two microfluidic geometries involving different materials were used during these experiments. The first geometry is a silicon−glass Y-shaped microdevice, as depicted in Figure 2 (Protron Mikrotechnik) that collects the two incoming fluids (H_2O, D_2O) and drives them into the same microchannel. The main channel is 500 μm wide, 40 μm deep, and a few centimeters long. The fluid handling is performed using custom-made connectics and commercial syringe pumps (Kd Scientific, KDS101).

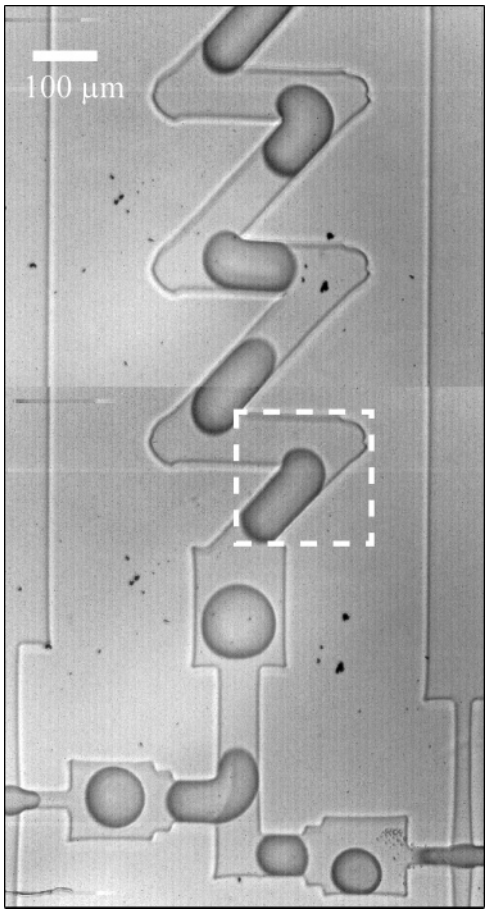

Figure 3. PDMS microreactor configuration for droplet generation. This image has been taken using a high-speed camera through a microscope (see text). H_2O (left) and D_2O droplets (right) are generated and coalesce in a carrier continuous silicone oil phase. The resultant droplets are transported throw a winding channel. H_2O and D_2O flow rates are equal to 75 μL/h. To ensure mother droplets synchronization, silicone oil flow rate is 90 μL/h on H_2O side and 100 μL/h on D_2O side. The white dashed square indicates the position of the measured Raman images displayed in Figure 7.

In this first series of experiments, H_2O and D_2O were injected in the two inlets of the device, at a same constant flow rate, ranging between 18 and 120 μL/h. The chemical exchange reaction is then followed in the main channel using a Raman spectrometer coupled with a confocal microscope (see Figure 2). At these small length scales and for the fluid velocities investigated, the flow is laminar in the central channel and the two liquids mix by molecular diffusion,[2] initiating the chemical reaction resulting in the formation of HOD.

The other microfluidic network we used is a microcoalescer made entirely out of PDMS. The channels (50 μm deep) are molded on a wafer built by standard soft lithography techniques[26] and then sealed on a glass slide. The complete setup has been described elsewhere,[27,28] and an image of the operating device is shown in Figure 3.

(26) Mcdonald, J. C.; Whitesides, G. M. *Acc. Chem. Res.* **2002**, *35*, 491.
(27) Link, D. R.; Grasland-Mongrain, E.; Duri, A.; Sarrazin, F.; Cheng, Z.; Cristobal, G.; Marquez, M.; Weitz, D. A. *Angew. Chem., Int. Ed.* **2006**, *45*, 2556
(28) Sarrazin, F.; Prat, L.; Miceli, N. D.; Cristobal, G.; Link, D. R.; Weitz, D. A. *Chem. Eng. Sci.* **2007**, *62*, 1042.

Briefly, it consists of generating pairs of droplets, each one containing a reactant, and forcing them to coalesce. The aqueous components H_2O and D_2O, which form the droplets, are first injected in separate channels. One species mother droplets are naturally generated at the intersection of each aqueous component with two silicone oil streams, as it is usual in hydrophobic PDMS channels.[29] Two electrodes connected to a current generator are plugged inside the channel at the entrance of the two solutions. A 100-V voltage is applied between those electrodes, under a low-intensity current smaller than 1 mA. The mother droplets are therefore polarized with opposite charges, which helps the synchronization and the coalescence.[27] In the absence of current, droplets do not coalesce because the time of contact is too short to drain the film between them. The continuous and dispersed phases' flow rates are equal to 190 and 150 μL/h, respectively, so that the daughter droplets are generated at a frequency of 180 Hz and are monodisperse with a volume of 0.23 nL. After the coalescence, they pass through a serpentine channel whose bend angles are equal to 45° and which significantly enhance the mixing efficiency within the droplets.[28,30,31] The channel width of this setup is 60 μm. The droplets are $L_d = 140$ μm long and are transported through the winding channel at a constant speed U_d equal to 4.8 cm s^{-1}.

D. Experimental Coupling of Microfluidics and Raman Confocal Imaging. (1) Experimental Setup. Raman measurements were carried out using a Labram HR (Jobin-Yvon) as shown in Figure 2. This confocal Raman spectrometer provides a way to record spectra from micrometer-sized regions of a sample, coincident with the illuminated spot, so that the Raman spectra originating from this precise region can be recorded without significant contributions from out-of-focus zones. Raman scattering was excited by an argon ion laser ($\lambda = 514.5$ nm), and the spectra were collected with a 3-cm^{-1} spectral resolution (grating 600 lines cm^{-1}). The microscope objective used for focusing the laser beam is the same that collects the Raman backscattered light. In the first set of experiments (Y-shaped glass−silicon chip), we used a 50× objective (NA = 0.55) providing roughly 1-μm^3 sampling volume. The acquisition times range between 0.5 and 1 s per point. In the second series of experiments, a 100× water immersion objective was used (NA = 1.00) giving a 1-μm^3 sampling volume and the acquisition time was 5 s. The droplet flow was visualized using a high-speed camera (Phantom V4.1, Vision Research, Inc.) mounted on the Raman microscope with a 10× objective to adapt the field of view (see ref 27 for details). Movies were acquired at a frequency of 2000 frames s^{-1} with an exposition time of 50 μs. The microchips were mounted on an automated motorized $x-y$ translation stage controlled by a computer. Raman spectra were obtained by raster scanning the chips at each point of a grid centered in the main channel.

(2) Spectrum Treatment. In all the performed experiments, and despite the confocal arrangement of our setup, interferences from the Raman spectra of the channel surrounding materials had to be considered in the Raman signal collected from the flowing fluids. Indeed, in the first series of experiments with the glass−silicon chips (Y-shaped geometry), we use 50× objective that gives an axial resolution of $2a \approx 15$ μm not small enough compare to the channel height $h = 40$ μm (Jobin-Yvon), to remove completely the silicon signal (see Figure 2). However, the Raman silicon spectrum is dominated by the 521-cm^{-1} line, which does not superimpose with the H_2O/D_2O stretching modes region. No pretreatments are applied to the recorded spectra to extract the molar fractions of H_2O, D_2O, and HOD. In the second series of experiments (droplet-based geometry), PDMS C−H symmetric and asymmetric stretching modes superimpose significantly to the H_2O/D_2O signal even with the use of a 100× water immersion objective that decreases significantly the out-of-focus signals of the reticulated PDMS ($2a \approx 5$ μm compared to $h = 40$ μm).[32] Indeed, since the Raman signal is continuously collected on a large number of droplets carried by a silicone oil stream, its contribution may be rather important. To extract the molar compositions from such data, the contribution of PDMS (reticulated and silicone oil) has to be effectively removed from the collected Raman spectra.

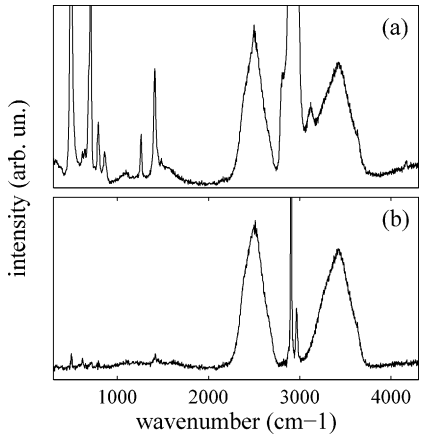

Figure 4. (a) Typical Raman spectrum I_{sample} measured in the case of the droplet flow: the raw signal is polluted by the PDMS signal. (b) Corrected spectrum I_{corr} used for molar composition quantification.

Figure 4a displays a typical spectrum measured in this configuration and clearly shows that the PDMS lines pollute the H_2O/D_2O streching modes. In order to remove the PDMS contribution from these recorded Raman spectra, we first focused on the 300−2000-cm^{-1} spectral range, which is mainly dominated by the PDMS signal. Note that the differences between the Raman spectra of reticulated PDMS and silicone oil are rather small and lie in the 580−650-cm^{-1} spectral region. By averaging 10 spectra obtained in the microchannel filled with silicone oil only, we obtained a typical in situ PDMS signal I_{PDMS}, incorporating all the optical effects associated to the microscope. Introducing two numerical constants β_1 and β_2, it is possible to generate for each measured spectrum I_{sample}, a corrected spectrum I_{corr}, free from the contribution of the PDMS signal. Such a couple (β_1, β_2) can be deduced by minimizing the difference $I_{sample} - \beta_1(I_{PDMS} + \beta_2)$ in the 300−2000-cm^{-1} range so that the corrected spectrum $I_{corr} = I_{sample} - \beta_1(I_{PDMS} + \beta_2)$ is obtained on the whole wavelength range. In this procedure, the coefficient β_2 accounts for baseline corrections whereas β_1 corrects the local intensity variations. We

(29) Thorsen, T.; Roberts, F. H.; Arnold, F. H.; Quake, S. R. *Phys. Rev. Lett.* **2001**, *86*, 4163
(30) Song, H.; Bringer, M. R.; Tice, J. D.; Gerdts, C. J.; Ismagilov, R. F. *Appl. Phys. Lett.* **2003**, *83*, 4664.
(31) Song, H.; Chen, D. L.; Ismagilov, R. F. *Angew. Chem., Int. Ed.* **2006**, *45*, 7336
(32) Jayes, L.; Hard, A.; Sene, C.; Parker, S.; Jayasooriya, U. *Anal. Chem.* **2003**, *75*, 742.

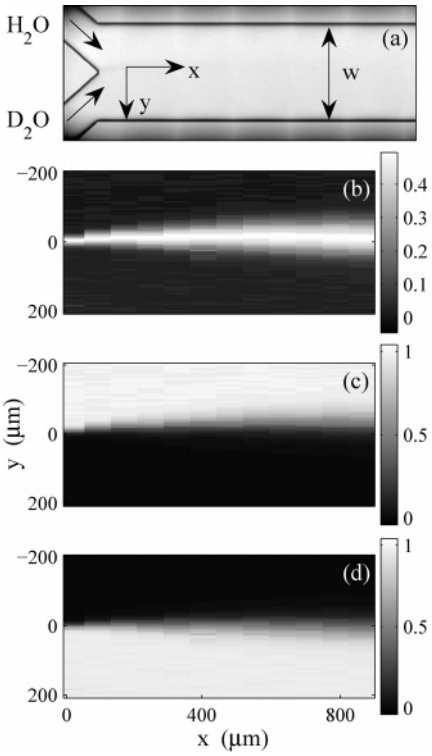

Figure 5. (a) Microscopic image of the silicon-glass Y-shaped microdevice (channel width $w = 500\ \mu$m). H_2O and D_2O are injected in the two arms of the chip at the same constant flow rate. Corresponding Raman images of (b) HOD, (c) H_2O, and (d) D_2O. The values correspond to the molar fractions of the three compounds deduced from the fitting procedure explained in the text. The three maps are not independent of each other. The flow rate in the main channel is 120 μL/h.

report in Figure 4b the result of this treatment: the corrected spectra can thus be fitted with the different experimental spectra showed in Figure 1 using the fitting procedure described previously in the 2250−2750- and 3150−3700-cm^{-1} ranges, since all the PDMS spectral contributions have been removed (the 3000-cm^{-1} PDMS line is still present on the corrected spectra as it saturated the detector).

RESULTS AND DISCUSSION

A. Interdiffusion and Reaction in the Coflow Configuration. We report results obtained on the Y-shaped chip for the case of a total flow rate $Q = 120\ \mu$L/h in the main channel. Typical Raman images displaying the molar fractions of H_2O, D_2O, and HOD are shown in Figure 5. They have been obtained from Raman spectra recorded on a 400 × 900 μm^2 grid (102 × 14 spectra) and treated according to the procedure detailed previously.

These three maps are not independant, but linked by eq 1 corresponding to the local chemical equilibrium. These maps clearly show that the H_2O/D_2O interdiffusion zone widens downstream and that HOD, the product of the reaction, appears in the diffusion zone. Interestingly, the diffusion zone is not perfectly symmetric: its center is located at $y \approx -20\ \mu$m. The width of the D_2O stream is wider than the H_2O one. Such an effect originates from the viscosity difference between the two injected fluids and has already been evidenced and discussed recently using the same setup for the case of the interdiffusion of nonreacting liquids.[22] Downstream the entrance length of the channel (of the order of the channel width w), and before the two fluids have significantly interdiffused, the widths of the incoming streams w_1 and w_2 are linked by $w_1/w_2 \approx \eta_1/\eta_2$, since both fluids are injected at the same flow rate. In our case, the viscosity of H_2O and D_2O are given respectively by $\eta_1 \approx 0.9$ and $\eta_2 \approx 1.1$ mPa·s at 25 °C,[33] leading to $w_1 \approx w/2 - 25\ \mu$m, consistent with our data.

We now concentrate on the quantitative analysis of these data. The Y-chip enables the parallel flow of H_2O and D_2O solutions in a microchannel: these two flowing solutions form an interdiffusion zone in which HOD appears. The reaction kinetics between H_2O and D_2O being very fast, reaction is diffusion-controlled and concentration maps of HOD only result from a diffusive process. If one considers a solute diffusing in a microchannel with a high aspect ratio $d << w$, its concentration profile $c(x,y)$ is a solution of

$$V\partial_x c(x,y) = D\partial_y^2 c(x,y) \tag{2}$$

where D is the diffusion coefficient of the solute and V the mean velocity of the flow. This description only holds in the case of the diffusion of a dilute solute (no coupling between the flow and the diffusion) and at high Péclet number $Pe = VD/d \gg 1$.[34,35] In the case of a point source initial condition, i.e., $c(x = 0,y) = c_0\delta(y)$, the concentration profile is given downstream by

$$c(x,y) = \frac{c_0}{\sqrt{4\pi D\tau}} \exp\left(-\frac{y^2}{4D\tau}\right) \tag{3}$$

with $\tau = x/V$. This expression for $c(x,y)$ may apply to our case and give, for each x position, the concentration profiles as a function of y. However, such a simplified analysis assumes uniform fluid viscosities in the channel and does not explicitly consider the chemical reaction. Instead of eq 3, we fitted the HOD concentration profiles at each location x downstream the microchannel by

$$c(y) \propto \exp\left(-\frac{(y - y_0)^2}{4\sigma^2}\right) \tag{4}$$

where σ and y_0 are both free parameters that depend on x. Note that eq 3 corresponds to this equation with $y_0 = 0$ and $\sigma = (Dx/V)^{1/2}$. The y_0 parameter has been introduced in order to account for the observed asymmetry of the Raman concentration maps. Equation 4 fits rather well all our data for the investigated range of flow rates, as can be seen in a typical example displayed in Figure 6a.

Moreover, by evaluating the various values of σ as a function of x, for different flow rates Q, Figure 6b shows that all the curves collapse when plotted against $\tau = x/V$, where $V = Q/(dw)$ is the mean velocity in the microchannel. Moreover, this data set

(33) Lide, D. R., Ed. *Handbook of Chemistry and Physics*; CRC Press: Boca Raton, FL, 2004−2005.
(34) Ismagilov, R. F.; Stroock, A. D.; Kenis, P. J. A.; Whitesides, G.; Stone, H. A. *Appl. Phys. Lett.* **2000**, *76*, 2376.
(35) Salmon, J.-B.; Ajdari, A. *J. Appl. Phys.* **2007**, *101*, 074902.

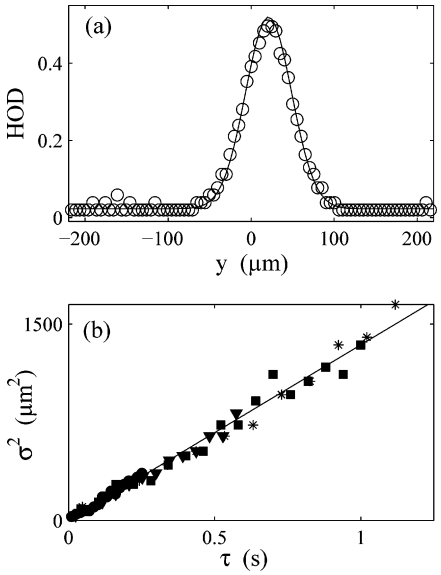

Figure 6. (a) Typical concentration profile of HOD, measured at $x = 170$ μm. The flow rate in the main channel is 36 μL/h. The continuous line is the best fit according to eq 4. (b) σ^2 vs $\tau = x/V$, where σ is deduced from the fits of the concentration profiles (see text for details). Different flow rates are plotted 36 (★), 60 (■), 120 (▼), and 240 μL/h (●). The continuous line is the best fit of the data according to $\sigma^2 = D\tau$ with $D = 1.3 \times 10^{-9}$ m^2 s^{-1}.

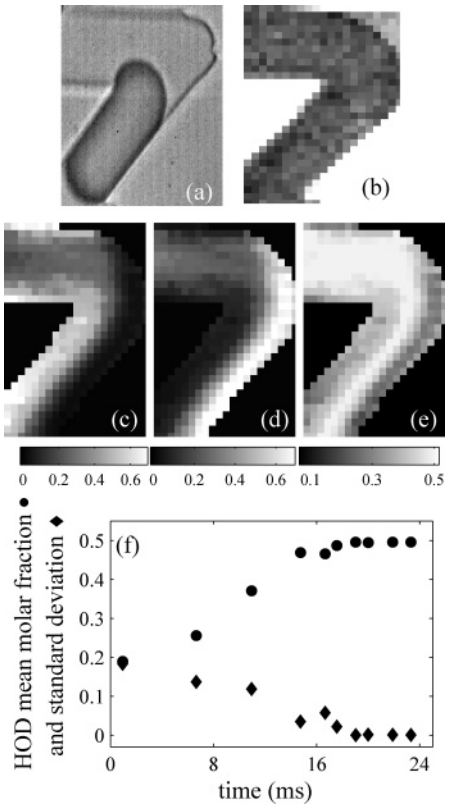

Figure 7. Images in the first bend crossed by the droplets (zone framed in Figure 3). (a) High-speed camera droplet snapshot. (b) PDMS signal: spectrum maximal intensity in the wave number range 580−650 cm^{-1} (arbitrary units, a linear gray scale codes for the Raman intensities). (c) H_2O, (d) D_2O, and (e) HOD molar fractions. All these images are 120 μm wide and 145 μm high. (f) Evolutions of the HOD mean molar fractions and standard deviations, as droplets flow through the channel (see text). The origin for the time t corresponds to the droplets coalescence instant.

suggests a simple diffusive behavior $\sigma^2 = D\tau$, with $D \approx 1.310^{-9}$ m^2 s^{-1}, which is a typical value of molecular diffusion coefficient. Note that the complete understanding of the interdiffusion of liquids with different viscosities is not the subject of this paper. It is unclear for us why such $\sigma^2 = D\tau$ behavior still holds in the case of liquids with different viscosities and, moreover, when a chemical reaction is involved.[22]

B. Mixing within Droplets. We now turn to the series of experiments performed using the PDMS microcoalescer device. As discussed previously for steady-state conditions, each location along the channel directly corresponds to a unique residence time after the droplet formation. It is thus possible to clock the phenomena hosted by the droplets by conveniently choosing the position in the channel where they are probed. One of the major advantages for implementing such chemical reactors is internal fluid recirculations within the droplets for fast and efficient mixing.[28,30] We focus on the effect of a 45° bend microchannel on the fluids' repartition within the droplet.

We show in Figure 3 the whole structure of the channel network: the white square inset captures the wiggly channel we consider (see the bright-field image in Figure 7a), which is the first bend channel crossed by the newly formed droplet after the coalescence.

Considering the Raman spectrum acquisition time being 5 s and the droplet production frequency being 180 Hz, each Raman spectrum recorded at a given location probes roughly an average signal over 900 droplets. Raman spectra were recorded every 5 μm on a spatial grid covering exactly the image given in Figure 7a: it took ~1 h to obtain the whole map. The Raman image in Figure 7b was formed by integrating the spectra in the 580−650-cm^{-1} range, which mainly corresponds to the reticulated PDMS Raman signature: the clear contrast between the bright parts (reticulated PDMS) and the dark regions shows that the sharp channel contours are well resolved by Raman imaging. We display in Figure 7c−e the average spatial distributions of H_2O, D_2O, and HOD molar fractions, as deduced from Raman images using the fitting procedure discussed earlier. The droplet flow being stationary, what we see on these images is nothing else but the evolution of the droplet composition along their progression within the channel. Note that, due to the droplet velocity ($U_d = 4.8$ cm s^{-1}) and the Raman acquisition time (5 s), the Raman signal originated from the droplets is averaged along directions parallel to the flow. The H_2O and D_2O Raman maps (Figure 7c,d) illustrate how the fluids hosted by the droplet behave while passing through a bend: H_2O, initially located in the inner bend, is progressively directed along the channel walls after the bend, while D_2O passes from the outer bend to the channel center. This rearrangement is characteristic of the chaotic advection generated inside the droplets by the winding geometry (see refs 30 and 31 for details). This phenomenon enhances mixing so that HOD production, initially located on the channel median plane at the reactants' interface, spreads into the whole channel section after the bend passage.

The droplet mixing evolution along the winding channel can be probed by evaluating the HOD molar fraction across the channel width, along lines perpendicular to the flow at various downstream positions, characteristic of different residence times.

These times originating from the droplet coalescence instant, i.e., the time $t = 0$, are readily obtained using the measured droplet velocity U_d and the measured downstream positions. More precisely, Raman spectra are collected every 2 or 5 μm on these downstream lines, and HOD molar fraction is evaluated using the fitting procedure described earlier, after the PDMS contribution has been subtracted as described. Its mean value and standard deviation, calculated along the lines, are plotted in Figure 7f. As the daughter droplets flow, the mean HOD concentration increases continuously: after ~20 ms it reaches the stable value of 0.495, typical of the expected concentration when isometric reactant volumes are mixed (the mother droplets have the same volume). Similarly, the standard deviation decreases to zero suggesting that the total mixing time, for the operating conditions considered, is ~20 ms. HOD mean molar fraction and its standard deviation across the channel width are good indicators of the mixing efficiency since they give information about the spatial heterogeneities of the concentration inside the drops; however, evolutions of other quantities (HOD molar fraction in the centerline of the droplets) are similar to the evolutions displayed in Figure 7f and lead to the same estimation of the mixing time. The estimated mixing time of 20 ms corresponds to a downstream distance of ~1 mm (the origin of time is set at the droplet coalescence instant), and it also corresponds roughly to five 45° bends.

We now focus on a more detailed analysis of the time required to homogenize droplet composition. Before attaining the channel bends, H_2O and D_2O are first both confined within one hemisphere of the droplets (half droplet). These two hemispheres are in contact through the channel median plan, and they mix slowly by diffusion.[23] After $t_1 = 7$ ms, the droplets enter the winding section, which enhances mixing efficiency. Indeed, Song et al. suggested that the droplet deformation and the fluid reorientation within the droplets after each bend induce an efficient mixing (the so-called chaotic advection) and that an estimate of the homogenization time may be obtained from $t_2 = (L_d/U_d)\ \ln(Pe)$, where Pe is the Péclet number given by $Pe = wU_d/D$.[30] Using for D the estimate obtained earlier ($D = 1.3 \times 10^{-9}$ m^2 s^{-1}), we obtain $t_2 =$ 10 ms, so that the total mixing time $t_1 + t_2$ appears in good agreement with our experimental evaluation.

CONCLUSIONS

Microfluidic devices are the roots of lab-on-a-chip systems whose most advanced designs can be used for sensors, for sample pretreatment, and for screening conditions of chemical conditions. A significant issue for the development of these approaches is to dispose reliable, selective, and sensitive probes to perform online chemical analysis from flowing systems. Among the possible analytical strategies, Raman confocal spectroscopy seems to offer great possibilities: its selectivity and spatial resolution in the micrometer range are very well adapted. In this study, we have demonstrated that obtaining Raman maps displaying spatially resolved concentration profiles of the chemical species, involved in a diffusion-controlled chemical reaction taking place in microfluidic systems, was straightforward. We investigated two typical microfluidic devices (diffusion-based and droplet-based systems), which are frequently used for probing chemical reactions. The acquition times of our Raman images were rather long (~1 h), but crucial to investigate mixing in these flows. For kinetic measurements only, one can perform Raman acquisitions at specific downstream locations where species are completely mixed. Furthermore, the low sensibility of Raman measurements is not a problem: flows being steady, spectra do not have to be time-resolved and can be obtained with long acquisition times and Raman enhancement effects (resonance and SERS) may also be used to increase significantly the measured spectra, and even probe individual droplets in specific microfluidic devices. The model chemical reaction we studied involves isotopic exchange between H_2O and D_2O: our results indicate it can be used for calibration purposes in other similar experiments involving Raman spectroscopy. This work paves the way for the implementation of chemiometric approaches in analyzing Raman data obtained with microfluidic devices. We also believe the method we describe in our work to remove the contributions of the silicone oil stream to the recorded spectra may be useful to investigate other chemical reaction in these droplet-based systems.

ACKNOWLEDGMENT

We thank A. Ajdari, M. Joanicot, B. Pavageau, and M. Yoda for fruitful discussions. We also acknowledge the Région d'Aquitaine for its financial support.

Received for review September 26, 2007. Accepted December 11, 2007.

AC7020147